Kohn-Luttinger Mechanism Driven Exotic Topological Superconductivity on the Penrose Lattice

Ye Cao,[1] Yongyou Zhang,[1] Yu-Bo Liu,[1] Cheng-Cheng Liu,[1] Wei-Qiang Chen,[2,3,4] and Fan Yang[1,*]
[1]School of Physics, Beijing Institute of Technology, Beijing 100081, China
[2]Department of Physics, Southern University of Science and Technology, Shenzhen 518055, China
[3]Shenzhen Institute for Quantum Science and Engineering, Southern University of Science and Technology, Shenzhen 518055, China
[4]Shenzhen Key Laboratory of Advanced Quantum Functional Materials and Devices, Southern University of Science and Technology, Shenzhen 518055, China

(Received 28 January 2020; revised 22 April 2020; accepted 15 June 2020; published 30 June 2020)

The Kohn-Luttinger mechanism for unconventional superconductivity (SC) driven by weak repulsive electron-electron interactions on a periodic lattice is generalized to the quasicrystal (QC) via a real-space perturbative approach. The repulsive Hubbard model on the Penrose lattice is studied as an example, on which a classification of the pairing symmetries is performed and a pairing phase diagram is obtained. Two remarkable properties of these pairing states are revealed, due to the combination of the presence of the point-group symmetry and the lack of translation symmetry on this lattice. First, the spin and spacial angular momenta of a Cooper pair is decorrelated: for each pairing symmetry, both spin-singlet and spin-triplet pairings are possible even in the weak-pairing limit. Second, the pairing states belonging to the 2D irreducible representations of the D_5 point group can be time-reversal-symmetry-breaking topological SCs carrying spontaneous bulk super current and spontaneous vortices. These two remarkable properties are general for the SCs on all QCs, and are rare on periodic lattices. Our work starts the new area of unconventional SCs driven by repulsive interactions on the QC.

DOI: 10.1103/PhysRevLett.125.017002

Introduction.—The quasicrystal (QC) has attracted a lot of research interests [1] since synthesized [2]. The QC represents a certain type of solid structures which are lack of translation symmetry but can possess rotation symmetries such as the fivefolded or eightfolded ones forbidden by crystalline point group [2]. The electronic structure on a QC is exotic and fundamentally different from that on a crystal. Specifically, due to the lack of translation symmetry on a QC, the lattice momentum is no longer a good quantum number and no Fermi surface (FS) can be defined. Various exotic quantum states with intriguing properties have been revealed on the QC recently [3–27]. Particularly, the definite experimental evidences for superconductivity (SC) in the recently synthesized Al-Zn-Mg QC [28], together with those in previous ternary QCs [29,30] and crystalline approximants [31], have attracted a lot of research interests [32–36]. It is interesting to ask a question here: are there any common features of superconducting states on the QC which are different from those on a crystal?

In Refs. [32,33,36], the pairing states for attractive Hubbard models are studied on QC lattices. It's found that the attractive interactions can lead to Cooper pairing [37] between a time-reversal (TR) partners, obeying the Anderson's theorem [38]. Further more, despite the lack of lattice momentum on the QC, the Cooper pairing can lead to a finite superfluid density [36]. These results [32,33,36] suggest that the SC on the QC with attractive interactions is consistent with the BCS theory. However, the situation is distinct for the cases with repulsive interactions, as will be shown below. The pairing in the presence of weak repulsive interactions is induced by the Kohn-Luttinger (KL) mechanism [39,40]. This theory states that the interaction renormalization brought about by exchanging particle-hole excitations is anisotropic on the FS, which can generate some attractive-interaction channels between the TR partners, which finally leads to Cooper pairing on the FS. Here, we generalize this mechanism to the QC, and obtain unconventional SCs with a series of remarkable properties intrinsic to the QCs which are rare on periodic lattices.

In this Letter, we study the KL SC in a weak-U repulsive Hubbard model on a Penrose lattice. Via a real-space perturbative treatment up to the second order, we acquire an effective interaction vertex, through which we derive a linearized gap equation near the superconducting critical temperature T_c, solving which we obtain the T_c and the pairing gap functions. We classify the pairing symmetries and obtain the pairing phase diagram after large scale numerical calculations. Two remarkable results are obtained. First, the orbital- and spin-angular momenta of the Cooper pair are decorrelated even without the spin-orbit

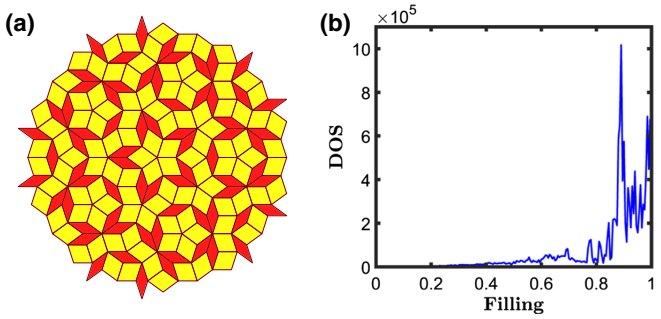

FIG. 1. Lattice pattern with 191 sites (a) and the DOS of the TB Hamiltonian on a lattice with 13 926 sites (b). In (a), the lattice constant is a.

coupling (SOC), which means that we can obtain both spin-singlet and spin-triplet pairings for the same pairing symmetry, distinguished from the case on a periodic lattice. Second, any 2D irreducible representation (IR) of the D_5 point group can bring about TR symmetry (TRS)-breaking topological SCs (TSCs) hosting spontaneous bulk super current and spontaneous vortices. These two properties are caused by the combination of the point-group symmetry and the lack of translation symmetry, and are thus general for the SCs on any QC, and are rare on periodic lattices.

Model and approach.—Let us consider the following standard repulsive Hubbard model on the Penrose lattice [41] with lattice constant a shown in Fig. 1(a) [42],

$$\hat{\mathcal{H}} = -\sum_{\mathbf{i},\mathbf{j},\sigma} t_{\mathbf{ij}} c^{\dagger}_{\mathbf{i}\sigma} c_{\mathbf{j}\sigma} + U\sum_{\mathbf{i}} n_{\mathbf{i}\uparrow} n_{\mathbf{i}\downarrow} - \mu \sum_{\mathbf{i},\sigma} n_{\mathbf{i}\sigma}, \quad (1)$$

where $c_{\mathbf{i}\sigma}$ annihilates an electron at site $\mathbf{i}$ with spin σ, $n_{\mathbf{i}\sigma}$ is the electron-number operator, and μ denotes the chemical potential. The hopping integral $t_{\mathbf{ij}} = e^{-|\mathbf{r_i}-\mathbf{r_j}|/\min(\{|\mathbf{r_i}-\mathbf{r_j}|\})}$, where $|\mathbf{r_i}-\mathbf{r_j}|$ denotes the distance between different sites $\mathbf{i}$ and $\mathbf{j}$, and $\min(\{|\mathbf{r_i}-\mathbf{r_j}|\}) = 0.618a$. The tight-binding (TB) part of Eq. (1) is diagonalized as $\hat{\mathcal{H}}_{\mathrm{TB}} = \sum_m \tilde{\epsilon}_m c^{\dagger}_{m\sigma} c_{m\sigma}$, with $c_{m\sigma} = \sum_{\mathbf{i}} \xi_{\mathbf{i}m} c_{\mathbf{i}\sigma}$. Here m labels a single-particle eigenstate with energy $\tilde{\epsilon}_m = \epsilon_m - \mu$ relative to the chemical potential, and $\xi_{\mathbf{i}m}$ represents for the wave function for the state m. The density of states (DOS) at the Fermi energy shown in Fig. 1(b) [43] peaks at around the filling fraction of 0.9, which will be focused on below. In unit of the largest hopping integral, the total band width W_D is about 7.56. We consider weak $U > 0$ and adopt perturbative approach in our work.

For this repulsive Hubbard model, SC is forbidden in the mean-field (MF) level. However, it can be driven by the KL mechanism, wherein unconventional SC is mediated by exchanging particle-hole excitations. Due to the lack of translation symmetry, we engage a real-space perturbative treatment, whose details are provided in the Supplemental Material [44]. The real-space propagator of the particle-hole excitations is described by the susceptibility function, which in the bare level reads [44]

$$\chi^{(0)}_{\mathbf{ij}}(i\Omega_n) = \int_0^{\beta} e^{i\Omega_n \tau} d\tau \langle T_\tau c^{\dagger}_{\mathbf{i}\uparrow}(\tau) c_{\mathbf{i}\uparrow}(\tau) c^{\dagger}_{\mathbf{j}\uparrow} c_{\mathbf{j}\uparrow}\rangle_0,$$
$$= \sum_{ml} \xi_{\mathbf{i}m}\xi_{\mathbf{j}m}\xi_{\mathbf{i}l}\xi_{\mathbf{j}l} \frac{n_F(\tilde{\epsilon}_m) - n_F(\tilde{\epsilon}_l)}{i\Omega_n + \tilde{\epsilon}_l - \tilde{\epsilon}_m}. \quad (2)$$

In our calculations, only about a 1000×1000 number of (m, l) near the Fermi level are summed in Eq. (2). In our perturbative treatment [44], the four second-order processes of exchanging particle-hole excitations induce effective interactions, from which we obtain [44]

$$\hat{\mathcal{H}}_{\mathrm{eff}} = -\sum_{\mathbf{i},\mathbf{j},\sigma} t_{\mathbf{ij}} c^{\dagger}_{\mathbf{i}\sigma} c_{\mathbf{j}\sigma} + U\sum_{\mathbf{i}} n_{\mathbf{i}\uparrow} n_{\mathbf{i}\downarrow} - \mu \sum_{\mathbf{i},\sigma} n_{\mathbf{i}\sigma}$$
$$- (U^2/2) \sum_{\mathbf{i},\mathbf{j},\sigma,\sigma'} \chi_{\mathbf{ij}} c^{\dagger}_{\mathbf{i}\sigma} c_{\mathbf{i}\sigma'} c^{\dagger}_{\mathbf{j}\sigma'} c_{\mathbf{j}\sigma}, \quad (3)$$

with $\chi_{\mathbf{ij}} \equiv \chi^{(0)}_{\mathbf{ij}}(i\Omega_n = 0)$. The induced term with coefficient $-(U^2/2)$ in Eq. (3) can drive SC in the MF level.

A BCS-MF study is performed on Eq. (3) [44]. Noting that the Cooper pairing can only take place near the Fermi level, we transform the real-space pairing order parameter $\Delta_{\mathbf{ij}}$ into the m space as $\tilde{\Delta}_{mn}$ and maintain those m/n states within a narrow energy shell near the Fermi level. A self-consistent MF equation for $\tilde{\Delta}_{mn}$ is obtained at any temperature, leading to the following linearized equation at T_c [44],

$$\sum_{m'n'} F_{mn,m'n'} \tilde{\tilde{\Delta}}_{m'n'} = \tilde{\tilde{\Delta}}_{mn}, \quad (4)$$

with $\tilde{\tilde{\Delta}}_{mn} = \tilde{\Delta}_{mn} f_{mn}$, where

$$f_{mn} = \sqrt{[n_F(-\tilde{\epsilon}_n) - n_F(\tilde{\epsilon}_m)]/(\tilde{\epsilon}_m + \tilde{\epsilon}_n)}. \quad (5)$$

The formula $F_{mn,m'n'}$ for the singlet pairing is given as

$$F^{(s)}_{mn,m'n'} = -f_{mn} f_{m'n'} \Big[U \sum_{\mathbf{i}} \xi_{\mathbf{i}m}\xi_{\mathbf{i}n}\xi_{\mathbf{i}m'}\xi_{\mathbf{i}n'}$$
$$+ \frac{U^2}{4} \sum_{\mathbf{i},\mathbf{j}} \chi_{\mathbf{ij}} (\xi_{\mathbf{i}m}\xi_{\mathbf{j}n} + \xi_{\mathbf{i}n}\xi_{\mathbf{j}m}) \times (m, n \Rightarrow m', n') \Big], \quad (6)$$

and for the triplet case it is

$$F^{(t)}_{mn,m'n'} = f_{mn} f_{m'n'}$$
$$\times \Big[\frac{U^2}{4} \sum_{\mathbf{i},\mathbf{j}} \chi_{\mathbf{ij}} (\xi_{\mathbf{i}m}\xi_{\mathbf{j}n} - \xi_{\mathbf{i}n}\xi_{\mathbf{j}m}) \times (m, n \Rightarrow m', n') \Big]. \quad (7)$$

The linearized gap equation (4) takes the form of an eigenvalue problem of the matrix $F_{mn,m'n'}$ (here we take the combined mn or $m'n'$ as one index), wherein its largest

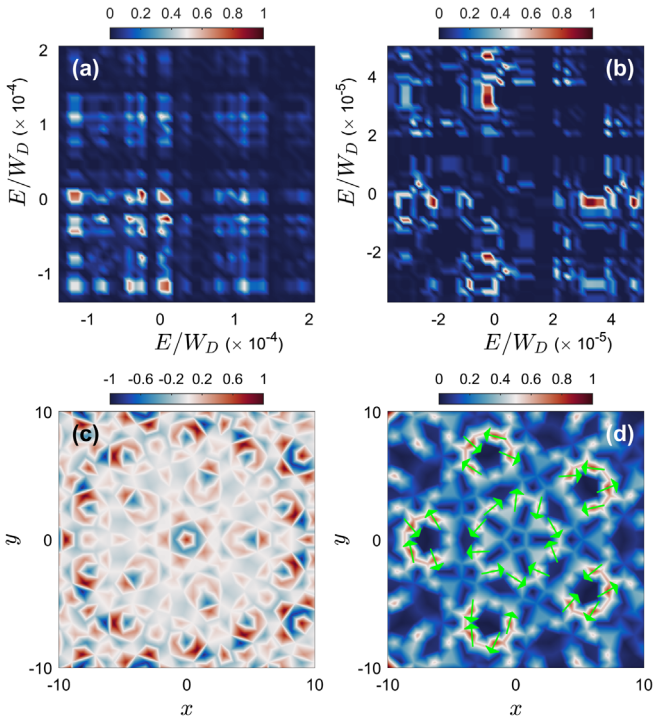

FIG. 2. Contour plots of relative $|\tilde{\Delta}_{mn}|$ and $\Delta_{\mathbf{i},\mathbf{O}}$, where $\mathbf{O}$ is the center of Penrose tiling, for a singlet s state [(a),(c) filling $= 0.81$, $U/W_D = 0.32$] and a triplet $d + id$ state [(b),(d) filling $= 0.98$, $U/W_D = 0.32$]. In (d), the direction of each marked green arrow at the site $\mathbf{i}$ represents phase angle of $\Delta_{\mathbf{i},\mathbf{O}}$ and the color represents the relative amplitude.

eigenvalue attains 1 at T_c, with the corresponding eigenvector $\tilde{\tilde{\Delta}}_{mn}$ determining the pairing symmetry. Due to the lack of translation symmetry here, the real-space gap function $\Delta_{\mathbf{i},\mathbf{j}}$ is no longer just a function of $\mathbf{i} - \mathbf{j}$, but a binary function of both $\mathbf{i}$ and $\mathbf{j}$. The situation is similar in the m space. The m, n dependence of $|\tilde{\Delta}_{mn}|$ is shown in Fig. 2 for two typical solutions solved from Eq. (4), where for each m there is no unique n which makes $|\tilde{\Delta}_{mn}|$ dominate that of any other n, distinct from the result for $U < 0$ wherein $|\tilde{\Delta}_{mm}| \gg |\tilde{\Delta}_{mn}(n \neq m)|$ [36]. Such a behavior breaks the Anderson's theorem applied for the strong-disorder-limit superconductors.

Pairing symmetries and phase diagram.—The classification of pairing symmetries here is based on the symmetry of the linearized gap equation (4) [44]. It is proved that the "pairing potential" $F_{mn,m'n'}$ is invariant under the D_5 point group. Consequently, the set of solutions $\{\tilde{\tilde{\Delta}}^{(\alpha)}_{mn}\}$ ($\alpha = 1$ or 1,2) of Eq. (4) corresponding to the same T_c furnish an IR of D_5. This statement also holds for the real-space gap function $\Delta^{(\alpha)}_{\mathbf{i},\mathbf{j}}$ [44]:

$$\Delta^{(\alpha)}_{\hat{g}\mathbf{i},\hat{g}\mathbf{j}} = \sum_{\alpha'} D^{(g)}_{\alpha\alpha'} \Delta^{(\alpha')}_{\mathbf{i},\mathbf{j}}, \tag{8}$$

with any $g \in D_5$. Then, from the IR which the set of matrices $\{D^{(g)}\}$ belong to, one can judge the pairing symmetry of the state with gap function $\Delta^{(\alpha)}_{\mathbf{i},\mathbf{j}}$.

The four IRs of the D_5 point group are listed in Table I, including two 1D IRs, i.e., A_1 and A_2, and two 2D IRs, i.e., E_1 and E_2. For each IR, we list the representation matrices for the two generators of D_5, i.e., the $C_{2\pi/5}$ and σ_x, up to an arbitrary unitary transformation. Each IR listed in Table I corresponds to one pairing-symmetry class. The identity representation A_1 is the s wave with angular momentum $l = 0$. The A_2 representation is the $h_{y^5-10x^2y^3+5x^4y}$ wave with $l = 5$ which is σ-reflection odd. The E_1 (E_2) representation provides the doubly degenerate p wave (d wave) with $l = 1$ ($l = 2$).

Note that for each of the pairing symmetry listed in Table I, both spin-singlet and spin-triplet pairings are possible, suggesting that the pairing angular momentum l and the spin statistics are independent. Such independence between the former and the latter is general on all QC lattices due to the lack of translation symmetry. Generally, in a singlet (triplet) pairing state where the spin part of the Cooper-pair wave function is exchange odd (even), the Fermi statistics requires the spacial part to be exchange even (odd). The exchange operation in the latter case can be viewed as a 180° rotation about the mass center of the Cooper pair, and thus this exchange parity is related to the angular momentum $\tilde{l}$ of the moving Cooper pair about its mass center. However, without translation symmetry, $\tilde{l}$ is different from l, as the latter is with respect to the fixed coordinate origin. Therefore, on QC lattices, the pairing

TABLE I. IRs of the D_5 point group and classification of pairing symmetries. $\hat{R}_\theta$ denotes the rotation about the center of the Penrose lattice by the angle $\theta = 2n\pi/5$ and $\hat{\sigma}$ represents the reflection about any of the five symmetric axes. $D^{(C_{2\pi/5})}$ and $D^{(\sigma_x)}$ are the representation matrices for the two generators of D_5, i.e., $C_{2\pi/5}$ and σ_x, up to any unitary transformation. For each pairing symmetry listed, both spin-singlet and spin-triplet pairings are possible.

IRs		$D^{(C_{2\pi/5})}$	$D^{(\sigma_x)}$	Pairing symmetries	Ground-state gap functions
1D	A_1	I	I	s	$\Delta_{\hat{R}_\theta\mathbf{i},\hat{R}_\theta\mathbf{j}} = \Delta_{\mathbf{i},\mathbf{j}}$, $\Delta_{\hat{\sigma}\mathbf{i};\hat{\sigma}\mathbf{j}} = \Delta_{\mathbf{i},\mathbf{j}}$
	A_2	I	$-I$	$h_{y^5-10x^2y^3+5x^4y}$	$\Delta_{\hat{R}_\theta\mathbf{i},\hat{R}_\theta\mathbf{j}} = \Delta_{\mathbf{i},\mathbf{j}}$, $\Delta_{\hat{\sigma}\mathbf{i};\hat{\sigma}\mathbf{j}} = -\Delta_{\mathbf{i},\mathbf{j}}$
2D	E_1	$\cos(2\pi/5)I \pm i\sin(2\pi/5)\sigma_y$	σ_z	(p_x, p_y)	$\Delta_{\hat{R}_\theta\mathbf{i},\hat{R}_\theta\mathbf{j}} = e^{\pm i\theta}\Delta_{\mathbf{i},\mathbf{j}}$, $\Delta_{\hat{\sigma}\mathbf{i},\hat{\sigma}\mathbf{j}} \neq \pm\Delta_{\mathbf{i},\mathbf{j}}$
	E_2	$\cos(4\pi/5)I \pm i\sin(4\pi/5)\sigma_y$	σ_z	$(d_{x^2-y^2}, d_{2xy})$	$\Delta_{\hat{R}_\theta\mathbf{i},\hat{R}_\theta\mathbf{j}} = e^{\pm 2i\theta}\Delta_{\mathbf{i},\mathbf{j}}$, $\Delta_{\hat{\sigma}\mathbf{i},\hat{\sigma}\mathbf{j}} \neq \pm\Delta_{\mathbf{i},\mathbf{j}}$

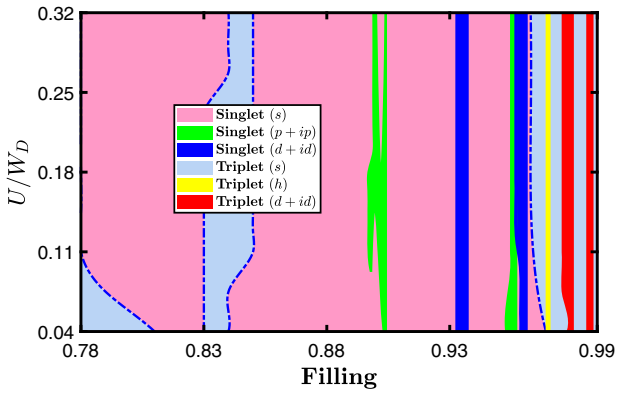

FIG. 3. Ground-state pairing phase diagram in the filling-interaction plane. The interaction strength of U is limited within a weak-coupling range of $(0, W_D/3)$.

angular momentum l and the spin statistics are unrelated. Note that such independence between the former and latter can also originate from the lack of inversion symmetry, which can also take place on noncentrosymmetric periodic lattices [45].

The pairing phase diagram is shown in Fig. 3 obtained through solving Eq. (4) for the singlet and triplet channels separately. In our calculations, we adopt a lattice with 13 926 sites with open-boundary condition. We focus on the filling range of (0.78,0.99) wherein the DOS is relatively large and the T_c is relatively high. The Hubbard-U adopted here is within a weak-coupling range of $(0, W_D/3)$. For the sake of reducing the computation complexity, we limit the states marked by $m^{(\prime)}/n^{(\prime)}$ in Eq. (4) to Eq. (7) within a narrow energy window near the Fermi level containing about 100 states. From Fig. 3, the obtained pairing symmetries slightly depend on U/W_D but strongly depend on the filling level. Six out of the eight possible pairing states listed in Table I are obtained, including the singlet and triplet s and d waves, the singlet p-wave and the triplet h-wave pairing symmetries.

Exotic TSCs.—The spin-singlet and spin-triplet p- and d-wave pairings states listed in Table I or Fig. 3 belong to 2D IRs of the point group, suggesting the existence of doubly degenerate gap functions $\Delta_{mn}^{(1,2)}$, which would be mixed below T_c to lower the free energy. At $T = 0$, the minimization of the expectation value of the effective Hamiltonian (3) in the BdG MF ground state with gap form factor $\Delta_{mn}^{(1)} + \alpha\Delta_{mn}^{(2)}$ yields $\alpha = \pm i$ for all these cases. Therefore such degenerate doublets would be mixed as $p + ip$ and $d + id$ in the ground state. The real-space gap functions $\Delta_{\mathbf{i},\mathbf{j}} = \Delta_{\mathbf{i},\mathbf{j}}^{(1)} \pm i\Delta_{\mathbf{i},\mathbf{j}}^{(2)}$ of these mixed states show nontrivial winding-number structures: with each θ-angle rotation ($\theta = 2n\pi/5$) about the lattice center performed on combined $(\mathbf{i}, \mathbf{j})$, the complex phase of $\Delta_{\mathbf{i},\mathbf{j}}$ would be shifted by $\pm l\theta$ (l: angular momentum), as listed in Table I, and shown in Figs. 2(c) and 2(d) for the s- and $(d + id)$-wave pairings, respectively. Such nontrivial winding numbers of these pairing states suggest that they are topologically nontrivial.

To better characterize the topology of these pairing states on the QC without translation symmetry [48,49], we use the K-theory class characterized by the Chern number. On the finite lattice, based on the spectral-localizer method, the Chern number is obtained as the following pseudospectrum invariant index C_{ps} [44],

$$C_{ps} = \frac{1}{2}\mathrm{Sig}\begin{pmatrix} X & Y + iH \\ Y - iH & -X \end{pmatrix}. \tag{9}$$

Here X and Y are the position operators, H is the BdG-Hamiltonian matrix and Sig represents the difference between the numbers of positive and negative eigenvalues of the matrix acted on [44]. Using this formula, we prove [44] that any global unitary transformation on the system maintains C_{ps}, and that the TR operation changes the sign of C_{ps}, which lead to the following conclusions. First, the C_{ps} of all 1D-IR pairing states are zero. Second, for triplet pairing states belonging to the 2D-IRs, the C_{ps} for the TRS-breaking chiral-pairing states $\sum_{\mathbf{ij}} \Delta_{\mathbf{i},\mathbf{j}}(c_{\mathbf{i}\uparrow}c_{\mathbf{j}\downarrow} + c_{\mathbf{i}\downarrow}c_{\mathbf{j}\uparrow}) + \mathrm{H.c.}$ [or $\sum_{\mathbf{ij}} \Delta_{\mathbf{i},\mathbf{j}}(c_{\mathbf{i}\uparrow}c_{\mathbf{j}\uparrow} \pm c_{\mathbf{i}\downarrow}c_{\mathbf{j}\downarrow}) + \mathrm{H.c.}$] are twice of those for the spinless system with $\sum_{\mathbf{ij}} \Delta_{\mathbf{i},\mathbf{j}}c_{\mathbf{i}}c_{\mathbf{j}} + \mathrm{H.c.}$, and those for the TRI helical-pairing states $\sum_{\mathbf{ij}}(\Delta_{\mathbf{i},\mathbf{j}}c_{\mathbf{i}\uparrow}c_{\mathbf{j}\uparrow} \pm \Delta_{\mathbf{i},\mathbf{j}}^{*}c_{\mathbf{i}\downarrow}c_{\mathbf{j}\downarrow}) + \mathrm{H.c.}$ are zero. These triplet pairing states are degenerate here without considering the spin-orbit coupling. Our numerical calculations on the 2D-IR singlet and chiral-triplet pairing states appearing in the phase diagram yield that their Chern numbers are generally integer multiples of twice of their spacial angular momenta, suggesting the presence of TSCs without translation symmetry.

A general and remarkable property of the TSCs on a QC is the presence of spontaneous bulk super current caused by the lack of translation symmetry. To illustrate this point, we have calculated the expectation values of the site-dependent current operator $\hat{\mathbf{J}}_{\mathbf{i}} = -\delta\hat{\mathcal{H}}/\delta\mathbf{A}_{\mathbf{i}}|_{\mathbf{A}=0} = (i/2)\sum_{\mathbf{j}\sigma} t_{\mathbf{ij}}(\mathbf{r}_{\mathbf{j}} - \mathbf{r}_{\mathbf{i}})c_{\mathbf{i}\sigma}^{\dagger}c_{\mathbf{j}\sigma} + \mathrm{H.c.}$ (see [44]). Note that $\hat{\mathbf{J}}_{\mathbf{i}}$ is TR odd, whose expectation value $\langle\hat{\mathbf{J}}_{\mathbf{i}}\rangle$ should vanish in TRI states. However, in the TRS-breaking chiral pairing states belonging to the 2D IR, our numerical results shown in Fig. 4 illustrate a fivefolded-symmetric pattern with $\langle\hat{\mathbf{J}}_{\mathbf{i}}\rangle \neq 0$ for any typical site. It is intriguing that the super current forms spontaneous vortices here and there, leading to bulk orbital magnetization that can be detected by experiments. Note that on periodic lattices, the spontaneous super current for a topological superconducting state usually appears at the edge [50–58], although it can also appear in the bulk on complex enough lattices. In the latter case, the averaged current within a unit cell should vanish, otherwise the superfluid density (see below) would be infinity. However, on the QCs with no translation symmetry

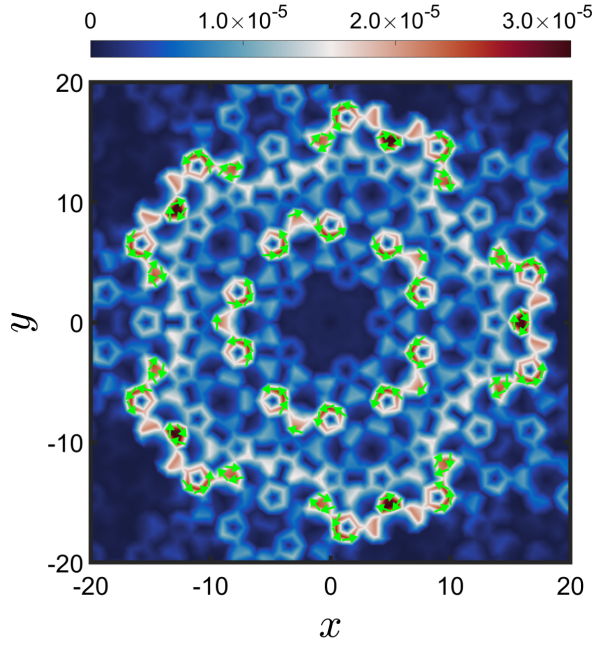

FIG. 4. Contour plot of the amplitude of the spontaneous bulk super current in the same pairing state as that in Fig. 2(b). The green arrows indicate the direction of the current at a specific site. To enhance the visibility, only typical sites are marked with the direction of the current.

and hence no unit cell, the distribution pattern of the super current is not limited by such a constraint.

Discussion and conclusion.—One might wonder whether the lack of translation symmetry on the Penrose lattice would destroy the phase coherence of the pairing state. This puzzle can be settled by investigating the superfluid density ρ_s defined as $\rho_s^{\alpha\beta} \equiv \lim_{\mathbf{A}\to 0}(-\langle \mathbf{A}|\hat{J}_\alpha[\mathbf{A}]|\mathbf{A}\rangle/A_\beta)$, with $\alpha/\beta = x, y$ [44]. Here a weak uniform vector potential $\mathbf{A}$ along the β direction is coupled with the system, $\hat{\mathbf{J}}[\mathbf{A}] = -\delta\hat{\mathcal{H}}[\mathbf{A}]/\delta\mathbf{A}$ and $|\mathbf{A}\rangle$ represents the ground state of $\hat{\mathcal{H}}[\mathbf{A}]$. It is proved here [44] that $\rho_s^{\alpha\beta} = \rho_0\delta_{\alpha\beta}$ and our numerical result yields $\rho_0 > 0$, suggesting a true superconducting state with nonzero superfluid density and hence measurable Meissner effect.

The real-space perturbative approach engaged here and the insight acquired from this Letter would also apply to other QCs. Particularly, the recently synthesized 30°-twisted bilayer graphene [59,60] provides a relevant platform for the QC Hubbard model studied here. Similar exotic TSCs would be detected there with proper doping. More interestingly, the D_{12} point group of that QC system leads to more IRs than those of the Penrose lattice. Consequently, exotic TSCs with winding numbers of 3, 4, and 5 are possible, higher than the 1 $(p+ip)$ or 2 $(d+id)$ obtained here or in periodic systems.

In conclusion, we have performed a real-space perturbative calculation for the Hubbard model on the Penrose lattice. Our results reveal various classes of unconventional SCs induced via the Kohn-Luttinger mechanism. We have classified the pairing symmetries according to the IRs of the D_5 point group of this lattice, with most of them exhibited in the pairing phase diagram. Remarkably, each pairing symmetry can be both spin-singlet and spin-triplet. All the 2D-IR pairing states can be TRS-breaking chiral TSCs hosting spontaneous bulk super current and spontaneous vortices. These pairing-mechanism-independent exotic properties of the SCs on the Penrose lattice are caused by the combination of the point-group symmetry and the lack of translation symmetry, and are thus general for all QC lattices, and are rare on periodic lattices. Our work starts the new area of unconventional SCs driven by repulsive interactions on the QC.

We acknowledge stimulating discussions with Wen Huang. This work is supported by the NSFC (Grants No. 11674025, No. 11704029, No. 11922401, No. 11674151, and No. 11774028).

*yangfan_blg@bit.edu.cn

[1] A. I. Goldman and R. F. Kelton, Quasicrystals and crystalline approximants, Rev. Mod. Phys. **65**, 213 (1993).
[2] D. Shechtman, I. Blech, D. Gratias, and J. W. Cahn, Metallic Phase with Long-Range Orientational Order and No Translational Symmetry, Phys. Rev. Lett. **53**, 1951 (1984).
[3] H. Tsunetsugu, T. Fujiwara, K. Ueda, and T. Tokihiro, Electronic properties of the Penrose lattice. I. Energy spectrum and wave functions, Phys. Rev. B **43**, 8879 (1991).
[4] H. Tsunetsugu and K. Ueda, Electronic properties of the Penrose lattice. II. Conductance at zero temperature, Phys. Rev. B **43**, 8892 (1991).
[5] S. Yamamoto and T. Fujiwara, Electronic transport of quasicrystals with random phason strain: The two-dimensional Penrose lattice, Phys. Rev. B **51**, 8841 (1995).
[6] S. Wessel, A. Jagannathan, and S. Haas, Quantum Antiferromagnetism in Quasicrystals, Phys. Rev. Lett. **90**, 177205 (2003).
[7] S. Thiem and J. T. Chalker, Long-range magnetic order in models for rare-earth quasicrystals, Phys. Rev. B **92**, 224409 (2015).
[8] A. Koga and H. Tsunetsugu, Antiferromagnetic order in the Hubbard model on the Penrose lattice, Phys. Rev. B **96**, 214402 (2017).
[9] J. Otsuki and H. Kusunose, Distributed hybridization model for quantum critical behavior in magnetic quasicrystals, J. Phys. Soc. Jpn. **85**, 073712 (2016).
[10] S. Watanabe and K. Miyake, Origin of quantum criticality in Yb–Al–Au approximant crystal and quasicrystal, J. Phys. Soc. Jpn. **85**, 063703 (2016).
[11] V. R. Shaginyan, A. Z. Msezane, K. G. Popov, G. S. Japaridze, and V. A. Khodel, Common quantum phase transition in quasicrystals and heavy-fermion metals, Phys. Rev. B **87**, 245122 (2013).
[12] N. Takemori and A. Koga, Local electron correlations in a two-dimensional Hubbard model on the Penrose lattice, J. Phys. Soc. Jpn. **84**, 023701 (2015).
[13] S. Takemura, N. Takemori, and A. Koga, Valence fluctuations and electric reconstruction in the extended Anderson

model on the two-dimensional Penrose lattice, Phys. Rev. B **91**, 165114 (2015).
[14] E. C. Andrade, A. Jagannathan, E. Miranda, M. Vojta, and V. Dobrosavljevic, Non-Fermi-Liquid Behavior in Metallic Quasicrystals with Local Magnetic Moments, Phys. Rev. Lett. **115**, 036403 (2015).
[15] Y. E. Kraus, Y. Lahini, Z. Ringel, M. Verbin, and O. Zilberberg, Topological States and Adiabatic Pumping in Quasicrystals, Phys. Rev. Lett. **109**, 106402 (2012).
[16] H. Huang and F. Liu, Quantum Spin Hall Effect and Spin Bott Index in a Quasicrystal Lattice, Phys. Rev. Lett. **121**, 126401 (2018).
[17] H. Huang and F. Liu, Comparison of quantum spin Hall states in quasicrystals and crystals, Phys. Rev. B **100**, 085119 (2019).
[18] S. Longhi, Topological Phase Transition in non-Hermitian Quasicrystals, Phys. Rev. Lett. **122**, 237601 (2019).
[19] S. Autti, V. B. Eltsov, and G. E. Volovik, Observation of a Time Quasicrystal and Its Transition to a Superfluid Time Crystal, Phys. Rev. Lett. **120**, 215301 (2018).
[20] K. Giergiel, A. Kuroś, and K. Sacha, Discrete time quasicrystals, Phys. Rev. B **99**, 220303(R) (2019).
[21] L.-J. Lang, X. Cai, and S. Chen, Edge States and Topological Phases in One-Dimensional Optical Superlattices, Phys. Rev. Lett. **108**, 220401 (2012).
[22] L. Sanchez-Palencia and L. Santos, Bose-Einstein condensates in optical quasicrystal lattices, Phys. Rev. A **72**, 053607 (2005).
[23] K. Singh, K. Saha, S. A. Parameswaran, and D. M. Weld, Fibonacci optical lattices for tunable quantum quasicrystals, Phys. Rev. A **92**, 063426 (2015).
[24] M. A. Bandres, M. C. Rechtsman, and M. Segev, Topological Photonic Quasicrystals: Fractal Topological Spectrum and Protected Transport, Phys. Rev. X **6**, 011016 (2016).
[25] J. Hou, H. Hu, K. Sun, and C. Zhang, Superfluid-Quasicrystal in a Bose-Einstein Condensate, Phys. Rev. Lett. **120**, 060407 (2018).
[26] D. Varjas, A. Lau, K. Pöyhönen, A. R. Akhmerov, D. I. Pikulin, and I. C. Fulga, Topological Phases without Crystalline Counterparts, Phys. Rev. Lett. **123**, 196401 (2019).
[27] S. Spurrier and N. R. Cooper, Kane-Mele with a twist: Quasicrystalline higher-order topological insulators with fractional mass kinks, arXiv:2001.05511.
[28] K. Kamiya, T. Takeuchi, N. Kabeya, N. Wada, T. Ishimasa, A. Ochiai, K. Deguchi, K. Imura, and N. K. Sato, Discovery of superconductivity in quasicrystal, Nat. Commun. **9**, 154 (2018).
[29] K. M. Wong, E. Lopdrup, J. L. Wagner, Y. Shen, and S. J. Poon, Transport and superconducting properties of the $Mg_{32}(Al,Zn_{49})$-type quasicrystalline and crystalline phases, Phys. Rev. B **35**, 2494(R) (1987).
[30] J. L. Wagner, B. D. Biggs, K. M. Wong, and S. J. Poon, Specific-heat and transport properties of alloys exhibiting quasicrystalline and crystalline order, Phys. Rev. B **38**, 7436 (1988).
[31] K. Deguchi, M. Nakayama, S. Matsukawa, K. Imura, K. Tanaka, T. Ishimasa, and N. K. Sato, Superconductivity of Au–Ge–Yb Approximants with Tsai-Type Clusters, J. Phys. Soc. Jpn. **84**, 023705 (2015).
[32] S. Sakai, N. Takemori, A. Koga, and R. Arita, Superconductivity on a quasiperiodic lattice: Extended-to-localized crossover of Cooper pairs, Phys. Rev. B **95**, 024509 (2017).
[33] R. N. Araújo and E. C. Andrade, Conventional superconductivity in quasicrystals, Phys. Rev. B **100**, 014510 (2019).
[34] S. Sakai and R. Arita, Exotic pairing state in quasicrystalline superconductors under a magnetic field, Phys. Rev. Research **1**, 022002(R) (2019).
[35] Y. Nagai, N-independent localized Krylov Bogoliubov-de Gennes method: Ultra-fast numerical approach to large-scale inhomogeneous superconductors, arXiv:2001.02362.
[36] Y.-Y. Zhang, Y.-B. Liu, Y. Cao, W.-Q. Chen, and F. Yang, Cooper instability and superconductivity on the Penrose lattice, arXiv:2002.06485.
[37] L. N. Cooper, Bound electron pairs in a degenerate fermi gas, Phys. Rev. **104**, 1189 (1956).
[38] P. W. Anderson, Theory of dirty superconductors, J. Phys. Chem. Solids **11**, 26 (1959).
[39] W. Kohn and J. M. Luttinger, New Mechanism for Superconductivity, Phys. Rev. Lett. **15**, 524 (1965).
[40] M. A. Baranov, A. V. Chubukov, and M. Y. Kagan, Superconductivity and superfluidity in fermi systems with repulsive interactions, Int. J. Mod. Phys. B **06**, 2471 (1992).
[41] R. Penrose, The role of aesthetics in pure, and applied mathematical research, Bull. Inst. Math. Appl. **10**, 266 (1974).
[42] Note that here we have set the center of the Perose lattice as the coordinate origin, and taken a symmetry-respected boundary to reflect the thermal-dynamic limit behavior.
[43] In the calculation of the DOS, we count the number N_E of the states locating within a narrow energy shell Δ_E near E_F, and the DOS is obtained as $N_E/N\Delta_E$, where N is the site number. Tune N and Δ_E, until a converged result of the DOS is obtained.
[44] See Supplemental Material at http://link.aps.org/supplemental/10.1103/PhysRevLett.125.017002 for our real-space perturbative theory on the repulsive Hubbard model, the basis for the classification of pairing symmetries on the QC, the definition and properties of the topological invariant, and the current operator.
[45] On a centrosymmetric periodic lattice without SOC, the pairing angular momentum l and the spin statistics are mostly mutually determined [46], particularly in the intra-band pairing case [47]. On a noncentrosymmetric lattice, a given irreducible representation of the point group does not possess definite parity of l. In this case, the parity of l is also independent from the spin statistics.
[46] M. Sigrist and K. Ueda, Phenomenological theory of unconventional superconductivity, Rev. Mod. Phys. **63**, 239 (1991).
[47] X.-L. Qi, T.-L. Hughes, and S.-C. Zhang, Topological invariants for the Fermi surface of a time-reversal-invariant superconductor, Phys. Rev. B **81**, 134508 (2010).
[48] T. A. Loring, K-theory and pseudospectra for topological insulators, Ann. Phys. (Amsterdam) **356**, 383 (2015).
[49] I. C. Fulga, D. I. Pikulin, and T. A. Loring, Aperiodic Weak Topological Superconductors, Phys. Rev. Lett. **116**, 257002 (2016).

[50] B. Horovitz and A. Golub, Superconductors with broken time-reversal symmetry: Spontaneous magnetization and quantum Hall effects, Phys. Rev. B **68**, 214503 (2003).

[51] M. Stone and R. Roy, Edge modes, edge currents, and gauge invariance in p_x+ip_y superfluids and superconductors, Phys. Rev. B **69**, 184511 (2004).

[52] B. Braunecker, P. A. Lee, and Z. Wang, Edge Currents in Superconductors with a Broken Time-Reversal Symmetry, Phys. Rev. Lett. **95**, 017004 (2005).

[53] J. A. Sauls, Surface states, edge currents, and the angular momentum of chiral p-wave superfluids, Phys. Rev. B **84**, 214509 (2011).

[54] C. Kallin, Chiral p-wave order in Sr_2RuO_4, Rep. Prog. Phys. **75**, 042501 (2012).

[55] W. Huang, E. Taylor, and C. Kallin, Vanishing edge currents in non-p-wave topological chiral superconductors, Phys. Rev. B **90**, 224519 (2014).

[56] K. D. Nelson, Z. Q. Mao, Y. Maeno, and Y. Liu, Odd-parity superconductivity in Sr_2RuO_4, Science **306**, 1151 (2004).

[57] J. R. Kirtley, C. Kallin, C. W. Hicks, E.-A. Kim, Y. Liu, K. A. Moler, Y. Maeno, and K. D. Nelson, Upper limit on spontaneous supercurrents in Sr_2RuO_4, Phys. Rev. B **76**, 014526 (2007).

[58] P. J. Curran, S. J. Bending, W. M. Desoky, A. S. Gibbs, S. L. Lee, and A. P. Mackenzie, Search for spontaneous edge currents and vortex imaging in Sr_2RuO_4 mesostructures, Phys. Rev. B **89**, 144504 (2014).

[59] S. J. Ahn, P. Moon, T.-H. Kim, H.-W. Kim, H.-C. Shin, E. H. Kim, H. W. Cha, S.-J. Kahng, P. Kim, M. Koshino, Y.-W. Son, C.-W. Yang, and J. R. Ahn, Dirac electrons in a dodecagonal graphene quasicrystal, Science **361**, 782 (2018).

[60] W. Yao, E. Wang, C. Bao, Y. Zhang, K. Zhang, K. Bao, C. K. Chan, C. Chen, J. Avila, M. C. Asensio, J. Zhu, and S. Zhou, Quasicrystalline 30° twisted bilayer graphene as an incommensurate superlattice with strong interlayer coupling, Proc. Natl. Acad. Sci. U.S.A. **115**, 6928 (2018).